

A new generation of effective core potentials: selected lanthanides and heavy elements

Haihan Zhou^{1, *} and Benjamin Kincaid¹, Guangming Wang¹,
Abdulgani Annaberdiyev², Panchapakesan Ganesh², and Lubos Mitas^{1,1}

¹*1) Department of Physics, North Carolina State University, Raleigh, North Carolina 27695-8202, USA*

*2) Center for Nanophase Materials Sciences Division,
Oak Ridge National Laboratory, Oak Ridge, Tennessee 37831, USA*

We construct correlation-consistent effective core potentials (ccECPs) for a selected set of heavy atoms and f -elements that are of significant current interest in materials and chemical applications, including Y, Zr, Nb, Rh, Ta, Re, Pt, Gd, and Tb. As customary, ccECPs consist of spin-orbit averaged relativistic effective potential (AREP) and effective spin-orbit (SO) terms. For the AREP part, our constructions are carried out within a relativistic coupled-cluster framework while also taking into objective function one-particle characteristics for improved convergence in optimizations. The transferability is adjusted using binding curves of hydride and oxide molecules. We address the difficulties encountered with f -elements, such as the presence of large cores and multiple near-degeneracies of excited levels. For these elements, we construct ccECPs with core-valence partitioning that includes $4f$ -subshell in the valence space. The developed ccECPs achieve an excellent balance between accuracy, size of the valence space, and transferability and are also suitable to be used in plane wave codes with reasonable energy cutoffs.

I. INTRODUCTION

Several years ago, we introduced correlation-consistent effective core potentials (ccECPs) that are constructed in an explicit many-body framework in contrast to more traditional one-particle approaches [1–5]. Our effort has been motivated by the use of valence-only calculations in both stochastic many-body methods such as quantum Monte Carlo (QMC) as well commonly used quantum chemistry approaches such as Configuration Interaction (CI) and Coupled Cluster (CC). Besides many-body constructions with overall high accuracy, this new generation of effective valence-only Hamiltonians also offers testing and benchmarking on molecular systems to boost the transferability for real chemical and material applications.

We have also established sets of reference data for constructed ccECPs, such as exact/nearly-exact total and kinetic energies and corresponding values typically obtained in single-reference real-space QMC calculations within the fixed-node approximation [6]. Similarly, our high accuracy QMC calculations of solids provided another set of transferability checks [7–9] in addition to other many-body calculations on large molecular complexes and solids carried out by independent groups [10–22]. We also probed the limits of systematic fidelity to all-electron results for $3sp$ main group elements with large cores that showed biases due to the absence of shallow core states in the valence space [2]. For example, significant biases were found for Al, Si, etc., with [Ne]-core in oxide molecules that show clear overbinding trends at smaller bond lengths. To overcome this limitation, we have also introduced small-core options with [He] instead of [Ne] cores [2]. Another aspect that has been

important in our effort is the issue of broad usability. For this purpose, accurate Gaussian basis sets have been provided. In addition, for plane-wave calculations with deeper semi-core states included in valence space, we offer another soft-ccECP version adapted for low cut-off in plane wave codes [23].

Here we present ccECPs for another selected set of elements, including transition metals, heavy elements, and, most importantly, a few lanthanides. It is well-known that the construction of ECPs for these elements is challenging due to several reasons, such as large relativistic effects including spin-orbit, many valence electrons, and also very large cores that can affect the transferability due to core polarizations and/or relaxations in varying chemical environments; difficult to resolve near-degeneracies showing up for states with occupations by $4f$, $5d$, $6s$ and $6p$ orbitals. Another issue is that there are much fewer calculations for heavy elements that probe the fidelity of ECPs in general, especially when compared with calculations involving elements from the first three rows [24–30]. For example, recent f -element calculations by Bauschlicher [31] show that some of the ECPs developed during the 1980s turned out to be less accurate than perhaps expected. One can see that the calculations are very sensitive to the choice of basis and that the resulting data can be significantly biased. This provides a clear motivation for revisiting this part of the periodic table with new generation ECP construction. In essence, our effort is focused on providing another alternative with better testing and benchmarking data from the outset to improve overall prospects of the constructed valence-only Hamiltonians. In this study, we opted for larger core sizes to clearly delineate the achievable accuracy of such a choice. Our well-tested construction can provide predictive power for many-body calculations across various applications regardless of minor compromises on the accuracy side.

In what follows, we briefly summarize the methods

* hzhou23@ncsu.edu

used. These are primarily based on our previous work [5]. We then describe the resulting operators, check the discrepancies of binding curves for hydride and oxide molecules, and make some overall accuracy comparisons with a summary of the results.

II. F-ELEMENTS CORE CHOICE

Obvious complexities for heavier atoms arise from the increasing number of electrons in the core resulting from filling the shells with higher principal numbers. This leads to the associated core and semi-core polarizability and relaxation effects, especially in the lanthanide row where f -electrons are involved. Although most of the f -electron charges are in the core region, the tails extend far beyond the nominal core radii and typically reach bonding regions [29, 30]. Hence, for $4f$ elements, an appropriate choice of the core size vs. valence space is less obvious. One possible choice is to decrease the core size to the innermost 28 electrons, i.e., all levels up to the principal quantum number $n = 3$. For such a choice of core the valence space will include several dozen electrons that leads to large total energies, which, unfortunately, makes it very costly to use methods such as QMC. Since core shells contributions scale as $\propto Z^2$ where Z is the atomic number, corresponding fluctuations decrease the QMC calculations, see, for example [32]. We note that overall QMC scaling on number of electrons N is very favorable $\mathcal{O}(N^2 \text{ to } N^3)$ [32], depending on details of the calculation. We also note that efficient coupled cluster algorithms with single, double and perturbative triple excitations scale as $\mathcal{O}(N^6 \text{ to } N^7)$ [33]. However, this favorable QMC scaling assumes a limited energy range (eg, valence band(s) states in a solid), otherwise the cost increases rapidly. For example, standard implementation of all-electron diffusion QMC for an atom scales as $\approx Z^{5.5}$, [32].

On the other hand, many constructions opt to use large cores, which also include f -electrons [24, 28, 30]. Although the resulting number of valence electrons is then small, which might be adequate for certain applications, the absence of the f -shell, especially in the middle of the lanthanide series, is problematic for many applications. In particular, lanthanides are some of the key elements for high-quality magnets where the large moments of the partially filled f -shell are crucial for properly describing magnetic properties. Since hybridization often changes the f -shell occupation, including these electronic states is essentially unavoidable in most materials calculations.

In our constructions, we attempt to balance accuracy and core size. Therefore, we have chosen to probe for a compromise solution that has been tested on the Tb element [34], namely using $5s5p4f$ one-particle levels in the valence for elements with partially filled f -subshells. This choice was less explored previously; for example, it was not included for lanthanides in the well-known Stuttgart-Koeln-Bonn energy consistent ECP table [35,

36]. Our work tests the viability of such core-valence partitioning with encouraging outcomes. In addition, we expect that this will be further ascertained in the future through more extensive calculations and tests.

III. METHODS

A. ECP form

The construction of our ECPs aims to reproduce valence properties of the all-electron Hamiltonian for given elements in a many-body, correlated framework. The form of the pseudopotentials follows the same parameterization as used in our previous works [3]. It consists of two parts, averaged relativistic effective potential (AREP) and corresponding spin-orbit (SO) terms:

$$V^{SOREP} = V^{AREP} + V^{SO}. \quad (1)$$

This can be further explicitly written as:

$$V^{AREP}(r) = V_{loc}(r) + \sum_{l=0}^{\ell_{max}=L-1} (V_l(r) - V_{loc}(r)) \sum_m |lm\rangle \langle lm| \quad (2)$$

Here the term V_{loc} represents the local potential, while $V_l - V_{loc}$ stands for the non-local s , p , d and f potentials with $\sum_m |lm\rangle \langle lm|$ as the angular-momentum projector. ℓ_{max} ranges from 3 to 4 depending on the element in question. V_{loc} is chosen to remove the Coulomb singularity from the potential. The local contribution is given as follows:

$$V_{loc}(r) = -\frac{Z_{eff}}{r}(1 - e^{\alpha r^2}) + \alpha Z_{eff} r e^{-\beta r^2} + \sum_{i=1}^2 \gamma_i e^{-\delta_i r^2} \quad (3)$$

where Z_{eff} is the number of electrons in the valence space. α , β , δ_i , and γ_i are all parameters optimized during the optimization. This form ensures the perfect cancellation of the Coulomb singularity and smoothes out the curvature of the potential at small r [37].

The non-local channels follow a similar form and are parameterized as given by

$$V_l(r) = \sum_{j=1} \beta_{\ell j} r^{n_{\ell j} - 2} e^{-\alpha_{\ell j} r^2} \quad (4)$$

where $n_{\ell j}$ are fixed integers determined prior to optimization, and $\alpha_{\ell j}$, $\beta_{\ell j}$ are parameters optimized for each non-local channel individually. Most functions in each channel have $n_{\ell j}$ equal to 2.

The spin-orbit terms are derived from Lee's definition of the general SOREP[38, 39] form. In our work, it is given by

$$V^{SO} = \sum_{l=1}^{l'_{max}} \Delta V_l P_l \vec{l} \cdot \vec{s} P_l \quad (5)$$

where l'_{max} is a chosen integer that indicates the number of channels of spin-orbit terms. \mathcal{P}_l is the same angular-momentum projector described above. The radial potential in the spin-orbit terms can be further parameterized as:

$$\Delta V_l = \sum_k \beta_{lk} r^{n_{lk}-2} e^{-\alpha_{lk} r^2} \quad (6)$$

Note that in both AREP and SO term constructions, the parameters n_{lj} and n_{lk} are usually chosen as integers and fixed during the process. The set of parameter α_{lj} , α_{lk} , β_{lj} and β_{lk} forms our parameter space. DONLP2[40], a sequential quadratic programming (SQP) algorithm based optimizer, is used to find the best combination of parameters with respect to the objective functions we constructed. For all the elements, we decided to find the best parameters of the spin-orbit terms after constructing the AREP ECP. As indicated in our previous work, the AREP part is most decisive regarding accuracy and transferability.

For Y, Zr, Nb, Rh, Ta, Re, and Pt, since the choice of their core is the same as the elements in the same row in our previous works, the objective functions and optimization process are similar. However, for Tb and Gd, the novel core choice also has led to extra complexities. To have a better starting point, two different initialization strategies have been experimented with before the legacy optimization workflow. The construction of objective functions in the legacy optimization routine will be introduced in the next section; Tb and Gd will be discussed shortly after.

B. Objective functions

The objective functions are crucial in constructing ECPs, as they directly reflect the desired properties to be reproduced. For the AREP ECP optimizations, the objective functions consist of several items. One of the important components is the minimization of atomic spectra discrepancies with respect to the ground state calculated at the CCSD(T) level. This includes the electron affinity (EA), several excited states, and ionization potentials (IPs) that aim to capture frequently observed effective charge states of the given atom in molecules and solids. Another useful criterium is reproducing the single-particle eigenvalues since they determine the tails of one-particle states and indirectly also the charge norm conservation. The objective function can be expressed as:

$$\mathcal{O}_{AREP}^2 = \sum_{s \in S} \omega_s (\Delta E_{ECP}^s - \Delta E_{AE}^s)^2 + \sum_{i \in I} \omega_i (\epsilon_{ECP}^i - \epsilon_{AE}^i) \quad (7)$$

Here ΔE^s represents the atomic gap of a state s with respect to the ground state in ECP and AE cases. Hence the first term indicates the sum of squared biases of the

chosen states from the AE atomic spectrum. The corresponding weight ω_s can be tuned to adjust the influence of each particular state, and having this flexibility improves the convergence of optimizations. ϵ^i represents the single-particle eigenvalue in ECP and AE cases. Usually, they correspond to the ground state, while $\{\omega_i\}$ are the corresponding weights. In our optimizations, $\{\omega_i\}$ are typically larger than $\{\omega_s\}$, with the difference reaching up to an order of magnitude to balance the impact of the terms that leads to faster optimization.

Here all the energies are obtained from CCSD(T) level calculations with large uncontracted basis sets, typically aug-cc-pwCVTZ with extra diffuse terms. For Gd and Tb, due to the sensitivity of the basis set choice, we have expanded the basis set to aug-cc-pwCVQZ with diffuse terms. All of our CCSD(T) calculations are carried out by Molpro v.2015.1 with 10th DKH Hamiltonian accounting for scalar-relativistic effects.

Very often, our ECP parameters are initialized from Stuttgart ECPs and further trained with the target objective functions. In some of the cases, we also tried to start with parameters from previous ccECPs of other elements, for example, in the same group or close in atomic number. Using this approach, Zr, Nb, Rh, Ta, and Re ECPs have been successfully constructed.

The spin-orbit terms are subsequently optimized after the AREP ccECPs are optimized and verified with transferability tests. Similar to the above, the objective function for the spin-orbit terms can be written as:

$$\mathcal{O}_{SO}^2 = \sum_{s \in S} \omega_s (\Delta E_{ECP}^s - \Delta E_{AE}^s)^2 + \sum_{m \in M} \omega_m (\Delta E_{ECP}^m - \Delta E_{AE}^m) \quad (8)$$

The main difference here is that instead of single-particle eigenvalues, we focus on the multiplet splitting energies referenced from the lowest energy of the same electronic state in ECP and AE cases, represented by ΔE^m . All the calculations for spin-orbit optimizations are carried out using the DIRAC code at the complete open-shell configuration interaction (COSCI) level of accuracy with the exact two-component Hamiltonian (X2C).

After the AREP and SOREP constructions are finalized, well-tempered (aug)-cc-p(C)VnZ basis sets ($n = D, T, Q, 5$ for non- f elements and D, T, Q for f -elements) are generated. The basis sets are optimized using the CISD method. We optimize the lowest exponent and the ratio between two subsequent exponents for each basis channel. After this procedure, the augmentation terms were added. More detailed explanations of basis set generations are given in the Supplementary Material.

C. ECP initialization of Tb and Gd

For the non- f elements, the initial parameters are often obtained from Stuttgart ECPs or previous ccECPs for other elements. However, due to the special choice of core for f -elements, namely $[\text{Kr}]4d^{10}$ (46 electrons), the initialization of ECP parameters becomes a non-trivial challenge. In the first place, we generate all the initial parameters from scratch. Additionally, in the complicated space formed by ECP parameters, numerous local minima can easily trap the optimization process if the initial guesses are not close enough to a desired or, at least, an acceptable local minimum.

For the Tb element, the initial guess generation can be summarized as follows:

1. Divide the collection of chosen states S into subsets S_i according to changing occupation in the channels with $i \in s, p, d, f$.
2. For each subset S_i , use a reduced objective function \mathcal{O}_{AREP}^i and optimize this single channel.
3. After all the non-local channels are independently optimized, combine all of them and initialize a local channel. Optimize the combined ccECP with the original objective function \mathcal{O}_{AREP} .

The primary gain here is reducing the number of parameters and the fact that the objective function \mathcal{O}_{AREP}^i contains only one single-particle eigenvalue. This makes the optimization process finish much faster than if there were more parameters and a more complicated objective function. The results for the Tb element will be shown in later sections.

However, it is not guaranteed that this will work for all cases of interest. This happens when the above procedure is applied to initialize the Gd element. After many restarts, we tried a slightly modified approach, which eventually worked as follows:

1. Partition the chosen set of states S into S_{sp} , S_d and S_f .
2. We optimize the S_{sp} objective function with extra single-particle eigenvalues from different states included, beyond just the ground state.
3. Add the d channel with initial guesses and update the modified reduced objective function with d -related atomic spectrum gaps so that spd channels are optimized.
4. Update the f channel and repeat step 3.

These additional optimization steps for the f -elements lead to a unique set of difficulties during ECP constructions. Currently, due to the complicated parameter space, we found that it is difficult to come up with a universal solution to the initialization problem of the f -elements. At the same time, since Tb and Gd have been generated successfully, as will be shown later, these can be used as possible starting points for other f -elements.

IV. RESULTS

For each element we demonstrate the accuracy of the spectrum in a table with three versions of absolute deviations related to the ECP gaps compared to the corresponding AE values. The first one is the mean absolute deviation (MAD). For the considered N atomic states, the MAD is defined as follows:

$$\text{MAD} = \frac{1}{N} \sum_{s=1}^N |\Delta E_s^{\text{ECP}} - \Delta E_s^{\text{AE}}|. \quad (9)$$

The next metric is the MAD of selected low-lying gaps for a smaller subset of n atomic states that includes only the states of the first excitation state (EX, mostly $s \leftrightarrow d$ transitions), electron affinity (EA), first ionization potential (IP), and second ionization potential (IP2):

$$\text{LMAD} = \frac{1}{n} \sum_{s=1}^n |\Delta E_s^{\text{ECP}} - \Delta E_s^{\text{AE}}|. \quad (10)$$

Additionally, a weighted MAD (WMAD) is defined as well for all considered N gaps as follows:

$$\text{WMAD} = \frac{1}{N} \sum_{s=1}^N \frac{100\%}{\sqrt{|\Delta E_s^{\text{AE}}|}} |\Delta E_s^{\text{ECP}} - \Delta E_s^{\text{AE}}|. \quad (11)$$

Besides our ccECPs, we calculate the same metrics for various other legacy ECPs for comparison. These ECPs include MWBSTU[41], MDFSTU[42, 43], CRENL[44, 45], SBKJC[46, 47], and LANL2[48]. Additionally, we present the results for uncorrelated core (UC) with correlated treatment restricted to valence subspace only (frozen-core). According to the above three defined metrics, MAD, LMAD, and WMAD, the summary of spectral comparison for each element is shown in Figures 1, 2, and 3.

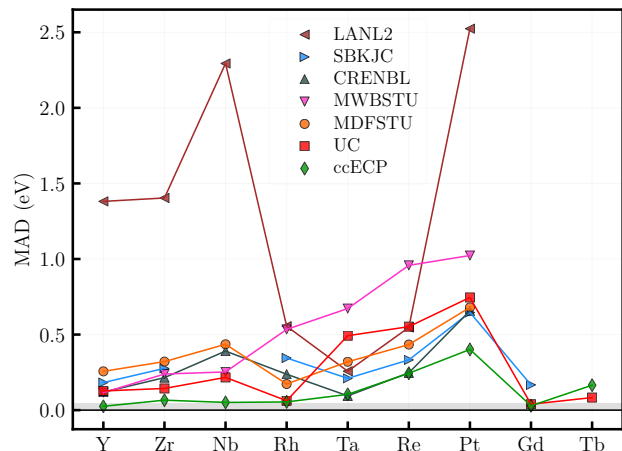


FIG. 1: Scalar relativistic AE gap MADs for various core approximations using RCCSD(T) method.

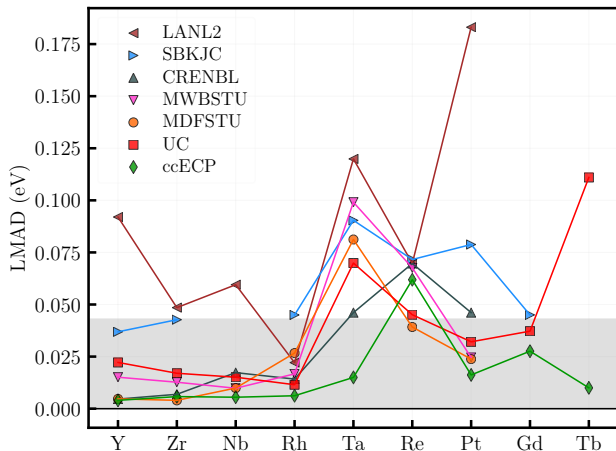


FIG. 2: Scalar relativistic AE gap LMADs for various core approximations using RCCSD(T) method.

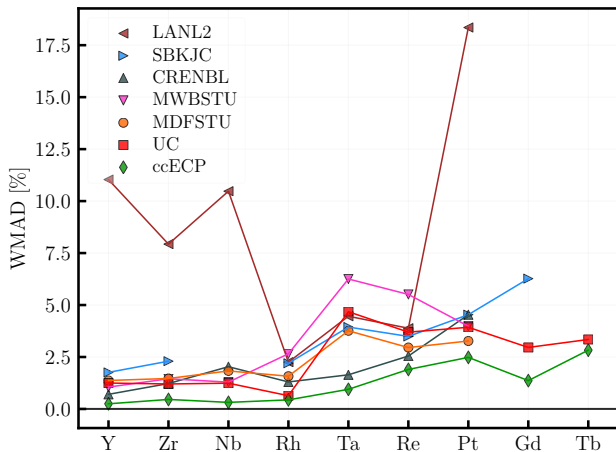


FIG. 3: Scalar relativistic AE gap WMADs for various core approximations using RCCSD(T) method.

For each element, we provide the transferability test of molecular binding energies for all core approximations compared to AE calculation with the fully correlated cores. In order to evaluate the quality of the ECPs, we utilize the discrepancy in dimer binding energies between the ECPs and AE calculations as given by

$$\Delta(r) = D^{ECP}(r) - D^{AE}(r) \quad (12)$$

where the $D(r)$ is the binding energy of dimer molecules at the atomic separation length r , which ranges from compressed bond length to stretched bond length. For each core approximation, the calculated binding energies are fitted to the Morse potential:

$$V(r) = D_e \left(e^{-2a(r-r_e)} - 2e^{-a(r-r_e)} \right), \quad (13)$$

where D_e denotes the dissociation energy, r_e labels the equilibrium bond length, and a is a fitting parameter

depends on the vibration frequency:

$$\omega_e = \sqrt{\frac{2a^2 D_e}{\mu}}, \quad (14)$$

where μ is the reduced mass of the molecule.

Table I, Table II, and Table III display the optimized parameters for the ccECPs pertaining to the selected elements of $4d$, $5d$, and $4f$ series, respectively.

A. Selected $4d$ elements

In this section, we discuss the results for Y, Zr, Nb, and Rh. The elements in this section use the same 28 electron core $[\text{Ar}]3d^{10}$ as in our previous ccECP work [5] with s , p , and d non-local channels. The SBKJC ECP was excluded for Nb in both atomic and molecular comparisons due to difficulties with CCSD(T) convergence. At the AREP level, the constructed ccECPs show significant improvement in terms of the accuracy of atomic spectra as shown in Figure 1, 2, and 3.

The binding energy discrepancy is plotted in a wide range of bond lengths, from near the dissociation limit at short distances to stretched bond lengths. We observe modest improvement in the binding curves of monohydrides and monoxides for these selected $4d$ elements. The results are shown in the following Figures 4, 5, 6, and 7.

We can observe that for Yttrium, given its simple structure, all the ECPs are presenting binding curves that are almost completely within the chemical accuracy bounds. We note that our ccECPs for Y, Zr, Nb, and Rh, show systematic improvements when compared to other ECPs. We see consistently small discrepancies at equilibrium bond lengths as well as throughout the entire bond lengths. Improvements are more noticeable in the oxide binding scenario, especially in ZrO and NbO, where ccECP outperforms other ECPs significantly to maintain accuracy in all geometries.

Our AREP ccECPs show systematic improvement when compared to legacy ECPs, both in atomic spectra and molecular tests. In Table IV, we provide the summary of mean absolute deviations for the binding parameters from the fit of the Morse potential. ccECP shows overall systematic consistency and a good balance between the imposed optimization criteria.

B. Selected $5d$ elements

This section includes elements Ta, Re, and Pt. The 60-electron core employed (configuration $[\text{Kr}]4d^{10}4f^{14}$) is identical to the core used for $5d$ elements from in our previous work [5].

The atomic spectra accuracy are presented with MAD, LMAD, and WMAD plots in Figures 1, 2, and 3, respectively. We observe consistent improvements in our ccECPs for Ta, Re, and Pt compared to other ECPs and

TABLE I: Parameters for the selected $4d$ atomic ccECPs. The highest ℓ value corresponds to the local channel L . The highest non-local angular momentum channel ℓ_{max} is related as $\ell_{max} = L - 1$.

Atom	Z_{eff}	Hamiltonian	ℓ	$n_{\ell k}$	$\alpha_{\ell k}$	$\beta_{\ell k}$	Atom	Z_{eff}	Hamiltonian	ℓ	$n_{\ell k}$	$\alpha_{\ell k}$	$\beta_{\ell k}$				
Y	11	AREP	0	2	6.868325	154.159199	Zr	12	AREP	0	2	8.765091	150.262314				
			0	2	3.830900	18.389590				0	2	3.928322	30.213713				
			1	2	6.193744	106.095839				1	2	7.417907	99.301910				
			1	2	2.739296	10.237893				1	2	3.768733	25.356026				
			2	2	5.301404	48.146429				2	2	2.250556	5.625707				
			2	2	2.236852	7.592843				2	2	5.355356	46.916833				
			3	1	11.322164	11.000000				3	1	23.999012	12.000000				
			3	3	15.695824	124.543799				3	3	25.971764	287.988139				
			3	2	5.067912	-20.049244				3	2	4.926614	-5.987178				
			3	2	4.444526	-5.929487				3	2	4.801388	-7.922580				
				SOREP	1	2	6.789339	-58.503206			SOREP	1	2	7.660616	-58.519285		
					1	2	6.773070	58.508207				1	2	7.440442	58.492385		
					1	2	3.078466	-7.554229				1	2	3.308537	-7.550185		
					1	2	2.896354	7.684825				1	2	3.147063	7.738905		
					2	2	5.419086	-11.851193				2	2	5.481717	-11.708397		
					2	2	5.333864	11.852624				2	2	6.090472	11.867706		
					2	2	1.970651	-2.065575				2	2	2.361902	-2.486771		
					2	2	1.954057	2.054659				2	2	1.764896	1.566729		
		Nb	13		AREP	0	2	8.451450	188.147277	Rh		17	AREP	0	2	11.968516	245.387919
						0	2	4.655854	25.673881					0	2	5.125760	27.285840
1	2			8.192024		134.298070	1	2	9.739600		180.589423						
1	2			3.466263		17.381556	1	2	6.564776		28.411628						
2	2			6.825072		60.151219	2	2	11.425921		83.487044						
2	2			2.858157		10.393369	2	2	4.502521		21.380372						
3	1			19.860892		13.000000	3	1	22.806206		17.000000						
3	3			19.525927		258.191591	3	3	32.710006		387.705494						
3	2			7.388201		-23.263128	3	2	14.048587		-10.571967						
3	2			4.558641		-4.887375	3	2	11.838335		-14.594461						
				SOREP	1	2	8.359425	-74.498506			SOREP	1	2	12.583835	-105.691011		
					1	2	8.167350	74.507443				1	2	9.850973	105.807831		
					1	2	3.685605	-10.879317				1	4	4.165404	-17.209011		
					1	2	3.551957	10.916537				1	4	6.179692	17.035664		
					2	2	6.688623	-15.214533				2	2	12.428318	-24.301306		
					2	2	6.537684	15.220185				2	2	14.006097	24.821099		
					2	2	2.551296	-3.000998				2	2	4.782894	-2.724934		
					2	2	2.557909	3.036924				2	2	5.952595	6.111212		

uncorrelated cores. For Ta, Re, and Pt, the MADs are clearly better than legacy ECPs. The LMAD for Tb is a little unique compared to the others shown. For Tb we were unable to converge an electron affinity state, so the calculation of the LMAD only includes the first excited state, first ionization potential, and second ionization potential. For low-lying states, Ta also shows significant improvement in the sense that all the other ECPs LMADs exceed the chemical accuracy, whereas ccECP achieves a comparable LMAD to that of some lighter transition metals. The LMADs for Re and Pt are also on par or better than the previous ECPs. Additionally, our ccECPs for

Ta, Re, and Pt show substantial improvements in terms of WMAD.

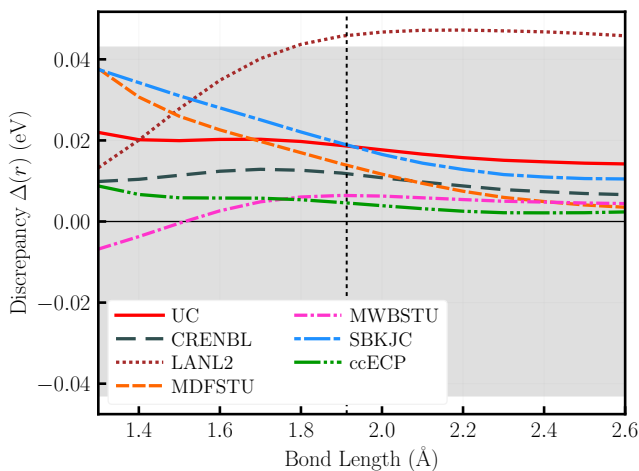
For the molecular calculation, similar to the $4d$ series, we also observed overall consistency and quality improvements shown in Figures 9, 8, and 10. For Re, the ReH and ReO ccECP binding curves are the only pair of curves that remain within the chemical accuracy across the range of bond length, with both ReH and ReO exhibiting noticeable improvements compared with other ECPs. It is worthwhile to mention that in ReO for UC, we exclude the molecular binding discrepancy curve near dissociation bond length due to the difficult convergence

TABLE II: Parameters for the selected $5d$ atomic ccECPs. The highest ℓ value corresponds to the local channel L . The highest non-local angular momentum channel ℓ_{max} is related as $\ell_{max} = L - 1$.

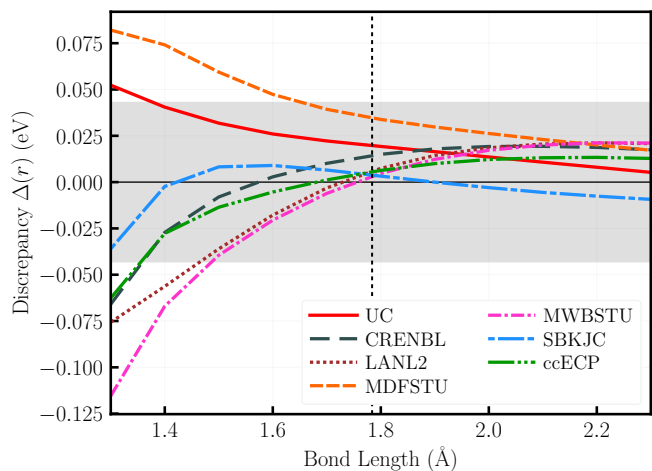
Atom	Z_{eff}	Hamiltonian	ℓ	$n_{\ell k}$	$\alpha_{\ell k}$	$\beta_{\ell k}$	Atom	Z_{eff}	Hamiltonian	ℓ	$n_{\ell k}$	$\alpha_{\ell k}$	$\beta_{\ell k}$	
Ta	13	AREP	0	2	16.084877	354.560780	Re	15	AREP	0	2	11.527415	471.040560	
			0	4	4.856689	-3.189062				0	2	3.521939	17.808887	
			0	2	6.308029	15.434060				1	2	9.670534	265.269318	
			0	2	4.049118	17.921890				1	2	4.693214	48.515418	
			1	2	9.219236	291.708719				2	2	6.202607	107.920979	
			1	4	8.304225	-10.543181				2	2	4.054883	31.437969	
			1	2	3.160451	-0.606327				3	2	2.502922	16.905644	
			1	2	2.276207	3.707560				3	2	4.013976	17.858142	
			2	2	5.663931	119.434072				4	1	13.992911	15.000000	
			2	4	6.804907	-1.428753				4	3	13.164906	209.893668	
			2	2	5.867466	6.084632				4	2	3.873316	-8.076852	
			2	2	5.458504	14.589293				4	2	3.654226	-9.999694	
			3	2	1.885697	13.741560								
			3	2	3.231234	12.967039				SOREP	1	2	9.196200	-176.980000
			4	1	6.585798	13.000000				1	2	9.692400	176.770000	
			4	3	9.131928	85.615374				1	2	7.722000	-20.947000	
			4	2	7.991861	-0.262937				1	2	3.956400	20.428000	
			4	2	1.842639	-2.273914				2	2	6.157000	-43.309000	
										2	2	6.201600	43.086000	
			SOREP	1	2	9.567757				-193.788022	2	2	4.608100	-5.345500
1	2	7.672453	195.894081	2	2	3.941100	5.715900							
1	4	9.284590	-9.653330	3	2	2.562700	-4.830900							
1	4	8.099739	6.253216	3	2	2.521500	4.830200							
1	2	3.637006	-0.144229											
1	2	1.690943	-1.601960	Pt	18	AREP	0	2	14.604490	428.400991				
2	2	5.498582	-45.969268	0			2	7.218055	67.391235					
2	2	5.595047	46.401258	0			2	5.429571	21.842450					
2	4	5.868634	-0.474343	1			2	11.178990	255.947773					
2	4	5.654115	0.293785	1			2	5.365413	52.709385					
2	2	1.414594	0.484404	1			2	8.011118	13.379362					
2	2	1.565152	-0.270081	2			2	7.615605	121.977058					
3	2	2.132660	-3.831108	2			2	3.904912	5.839996					
3	2	2.032923	3.924549	2			2	5.446875	44.746892					
				3			2	3.386257	13.308218					
				3			2	3.326489	19.517395					
				3			2	5.430616	25.350338					
				4			1	13.600000	18.000000					
				4			3	13.600000	244.800000					
				4			2	13.600000	-161.707117					
				4			2	5.430186	-19.530044					
				SOREP			1	2	12.905978	-176.006816				
				1			2	9.569534	176.041345					
				1			2	5.241937	-27.260853					
				1			2	7.370807	27.417143					
				2	2	8.156923	-42.598141							
				2	2	7.160691	44.200769							
				2	2	3.611191	-6.876859							
				2	2	4.034286	7.580091							
				3	2	3.379869	-7.140146							
				3	2	3.326255	7.139063							

TABLE III: Parameters for the selected $4f$ atomic ccECPs. The highest ℓ value corresponds to the local channel L . The highest non-local angular momentum channel ℓ_{max} is related as $\ell_{max} = L - 1$.

Atom	Z_{eff}	Hamiltonian	ℓ	$n_{\ell k}$	$\alpha_{\ell k}$	$\beta_{\ell k}$	Atom	Z_{eff}	Hamiltonian	ℓ	$n_{\ell k}$	$\alpha_{\ell k}$	$\beta_{\ell k}$						
Gd	18	AREP	0	2	11.958743	158.751573	Tb	19	AREP	0	2	8.996757	161.119164						
			0	2	4.575020	75.338628				0	2	5.104371	89.334835						
			1	2	9.327027	85.299703				1	2	7.640657	88.693021						
			1	2	3.727309	55.148896				1	2	3.878305	57.109488						
			2	2	9.142398	55.315114				2	2	7.456305	55.901690						
			2	2	2.410263	27.587515				2	2	2.530445	29.364333						
			3	2	3.496091	-24.952915				3	2	4.939345	-23.952530						
			3	2	6.162299	-2.920504				3	2	3.912490	-7.090915						
			4	1	4.482335	18.000000				4	1	4.526254	19.000000						
			4	3	4.564890	82.168015				4	3	3.879308	85.998831						
			4	2	5.667120	-92.949026				4	2	4.406058	-85.722649						
			4	2	3.161461	-4.588504				4	2	1.899664	-3.133952						
					SOREP	1				4	2.002999	2.782860			SOREP	1	4	2.080465	2.963688
						2				4	4.114860	-0.322458				2	4	2.660751	0.922456
			3	4	4.965905	0.231259				3	4	4.708055	0.178089						



(a) YH binding curve discrepancies



(b) YO binding curve discrepancies

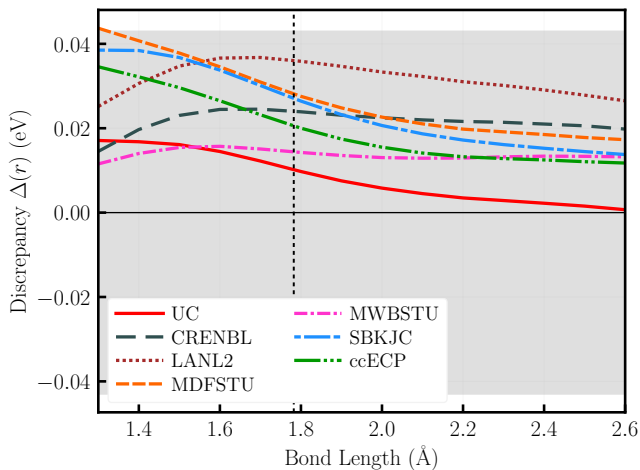
FIG. 4: Binding energy discrepancies for (a) YH and (b) YO molecules. The grey-shaded region indicates the chemical accuracy, and the vertical dashed line gives the equilibrium bond length from the AE result.

in the coupled cluster calculations. The uncorrelated core shows notable underbinding at short bond lengths. We conjecture that this is caused by the rigidity of $4f$ orbitals with long tails that reach the bonding region. This suggests that the correlations related to this subspace need to be captured, at least indirectly. For Ta, the TaH binding curve is on par with MDFSTU and MWBSTU, consistently within the chemical accuracy for the entire bond length range. For TaO, ccECP binding curve shows better accuracy, especially at the equilibrium bond length, while alleviating the overbinding issue in LANL2, MDFSTU, and CRENBL. For Pt, it is evident that our ccECP, alongside MDFSTU, outperforms other candidates across

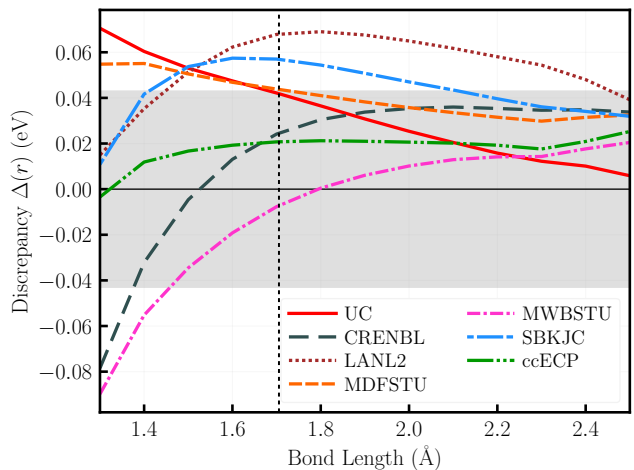
the entire bond length range.

It is important to note that throughout the optimization of the $5d$ elements, we imposed additional restrictions on the range of all exponents ($\alpha_{\ell k}$) to prevent high plane wave cutoffs in codes with periodic boundary conditions. Consequently, some compromises observed in the results stem from these additional restrictions made in favor of wider applicability in plane wave applications.

In conclusion, our ccECPs for the selected $5d$ elements, Ta, Re, and Pt, exhibit systematic improvements in both atomic spectra accuracy and molecular binding curves.

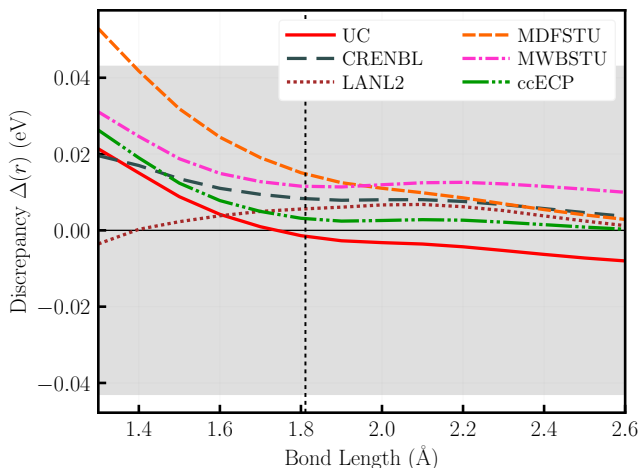


(a) ZrH binding curve discrepancies

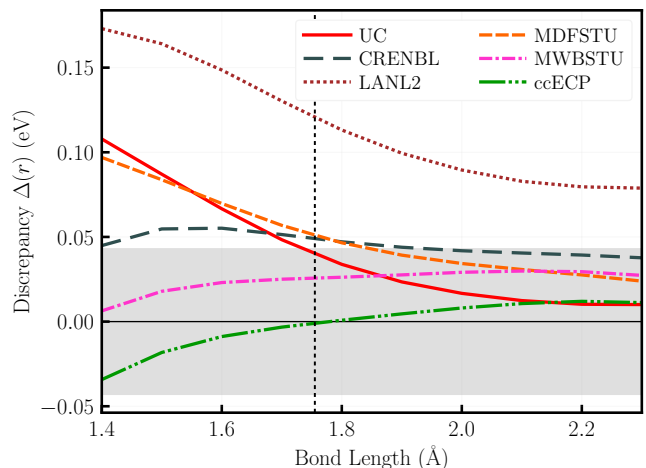


(b) ZrO binding curve discrepancies

FIG. 5: Binding energy discrepancies for (a) ZrH and (b) ZrO molecules. The grey-shaded region indicates the chemical accuracy, and the vertical dashed line gives the equilibrium bond length from the AE result.



(a) NbH binding curve discrepancies



(b) NbO binding curve discrepancies

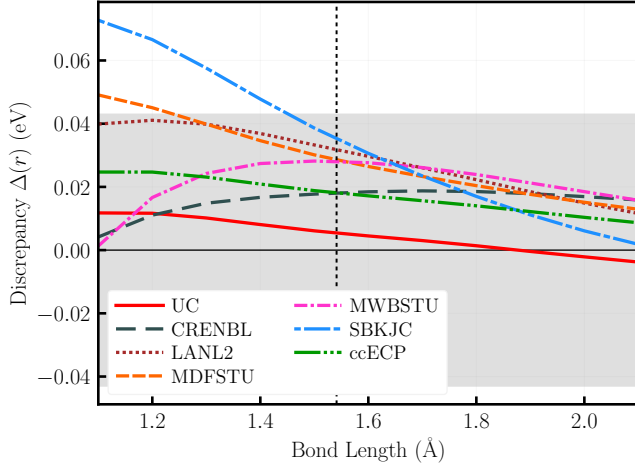
FIG. 6: Binding energy discrepancies for (a) NbH and (b) NbO molecules. The grey-shaded region indicates the chemical accuracy, and the vertical dashed line gives the equilibrium bond length from the AE result.

C. Selected $4f$ elements

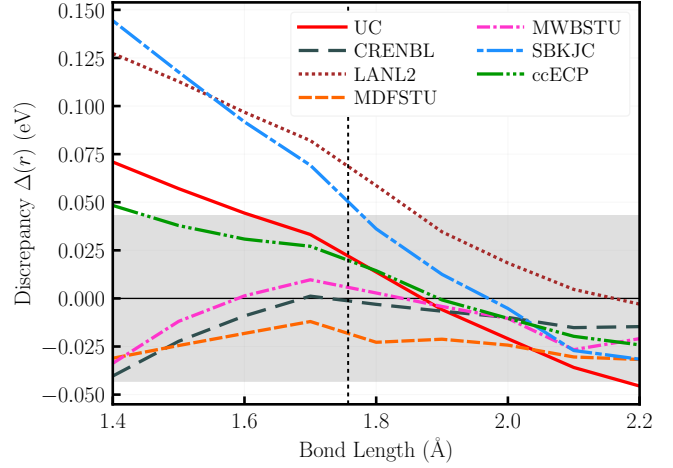
The elements in this section are characterized by a unique core configuration, which represents one of the novel aspects of this work. The core comprises 46 electrons, separating thus the $n = 4$ shell into subshells. Specifically, the core is given as $[[\text{Kr}]4d^{10}]$, with the $4f$ subshell included in the valence space. This unorthodox core choice has been less explored in previous ECP constructions since the core is often defined by a closed shell of principal quantum number n . For instance, the core for $3d$ transition metals includes electrons up to $n = 2$ ($[\text{Ne}]$ -core), while for the $4d$ transition metals it is $n = 3$

($[\text{Ar}]3d^{10}$).

Generating ECPs for these elements required a modified approach due to the chosen core structure. We first fitted eigenvalues for each one-particle channel to establish reliable initial guess parameters. A similar procedure of developing initial guess parameters has been applied in our previous work when constructing soft ccECPs for the late $3d$ transition metals [23], and an analogous initialization was originally proposed by Dolg et al. [49]. We refer the reader to Section III C for details of ECP parameter initialization descriptions. The subsequent optimization procedure follows a similar scheme to our previous work, where the energy gaps for various states served as

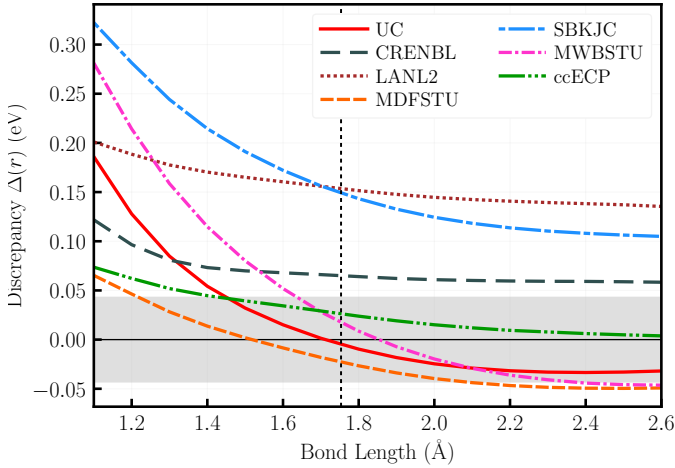


(a) RhH binding curve discrepancies

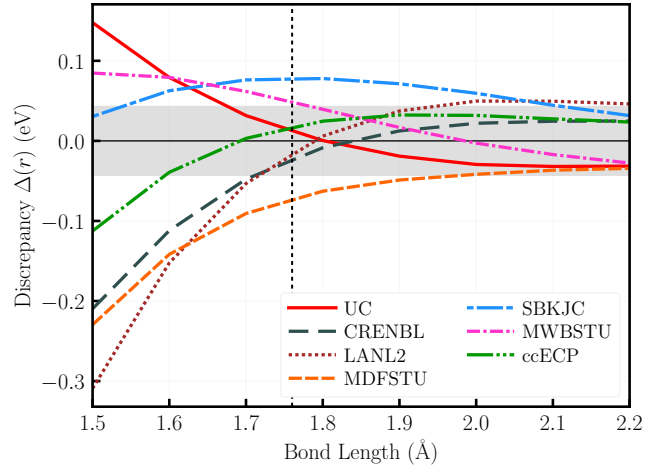


(b) RhO binding curve discrepancies

FIG. 7: Binding energy discrepancies for (a) RhH and (b) RhO molecules. The grey-shaded region indicates the chemical accuracy, and the vertical dashed line gives the equilibrium bond length from the AE result.



(a) TaH binding curve discrepancies



(b) TaO binding curve discrepancies

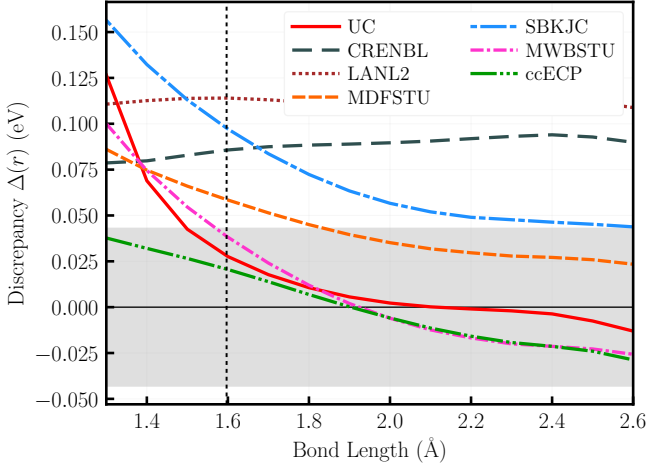
FIG. 8: Binding energy discrepancies for (a) TaH and (b) TaO molecules. The grey-shaded region indicates the chemical accuracy, and the vertical dashed line gives the equilibrium bond length from the AE result.

the objective function for optimization, iterated until the desired accuracy for the atomic spectrum was achieved. Thereafter, we performed the molecular transferability tests and made adjustments to obtain the best possible balance between atomic spectrum accuracy, molecular binding curve accuracy, and plane wave cutoffs as an additional criterium. Compared to previous sets of heavier elements [5], we used a smaller number of highly-ionized states due to the substantial difficulties they have caused in the optimization process.

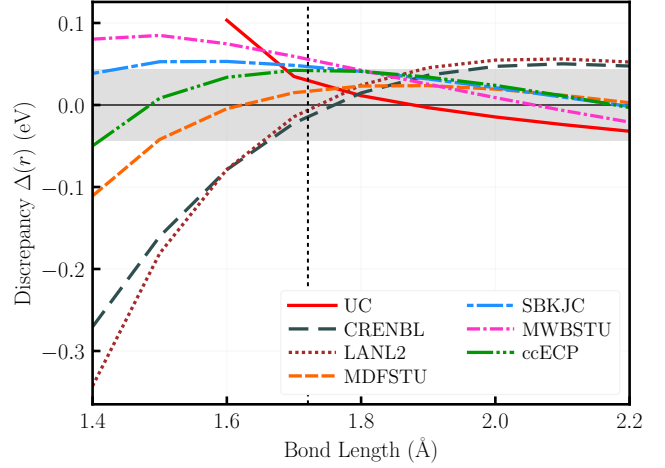
Despite the additional constraints applied to exponents (α_{lk}) for a desirably small cutoff in plane wave applications, our ccECP atomic results for Tb display com-

parable accuracy with the uncorrelated core results and show a significant improvement over SBKJC and also DFT-PBE (which was generated using Troullier-Martins scheme [50] and PBE functional [51]) in MAD, LMAD, and WMAD characteristics. In the case of Gd, the atomic results are again comparable to the UC results. As also observed for Tb, the UC atomic spectra accuracy is surprisingly high and very challenging to reach in our optimizations. This may indicate that our ccECP for Gd is probably approaching the fidelity limit of the presented construction.

For transferability tests of rare-earth elements (R), we focused on RH_3 and RO molecules, instead of regular

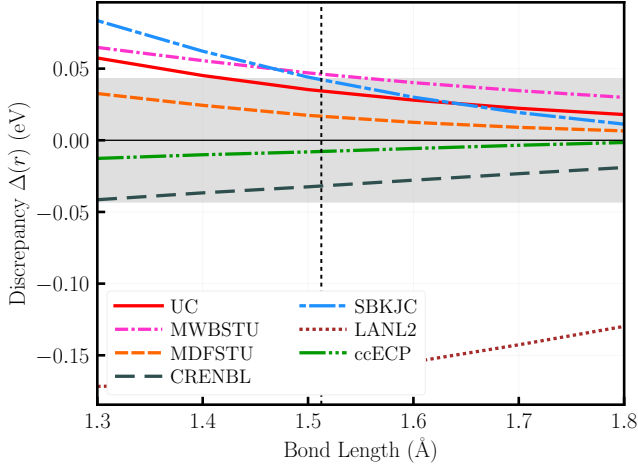


(a) ReH binding curve discrepancies

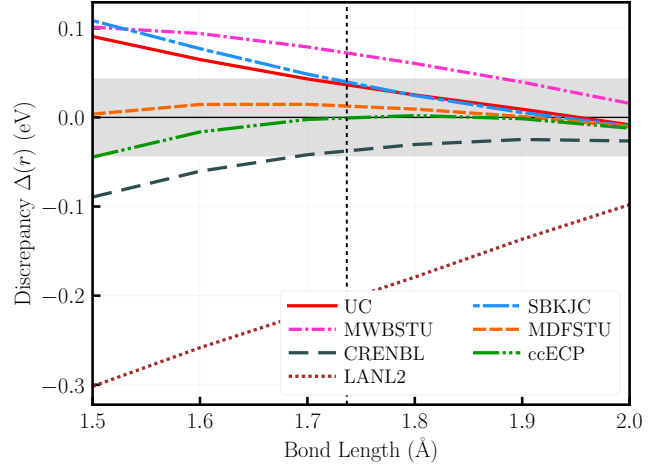


(b) ReO binding curve discrepancies

FIG. 9: Binding energy discrepancies for (a) ReH and (b) ReO molecules. The grey-shaded region indicates the chemical accuracy, and the vertical dashed line gives the equilibrium bond length from the AE result.



(a) PtH binding curve discrepancies



(b) PtO binding curve discrepancies

FIG. 10: Binding energy discrepancies for (a) PtH and (b) PtO molecules. The grey-shaded region indicates the chemical accuracy, and the vertical dashed line gives the equilibrium bond length from the AE result.

monohydride and monoxide molecules since the R^{2+} and R^{3+} are more relevant for wider applications, such as in bulk materials. The results are summarized in Figures 11 and 12. For both TbH_3 and TbO , our ccECP is clearly surpassing the legacy ECPs in quality and is comparable to the UC treatment. For most of the bond lengths, GdH_3 ccECP binding curves are within the chemical accuracy with minor compromises compared to UC calculations. Overall, our tests demonstrate successful, high-accuracy ccECP generation viability for rare-earth elements, utilizing Gd and Tb and the core choice that hasn't been systematically explored before. In addition, we find that the accuracy of UC is unexpectedly high in

Gd and Tb, which is at odds with some previous observations such as large core Na-Ar elements where ccECP accuracy was considerably better than UC [2].

We note that further studies are still needed to better understand Gd, Tb, and rare-earth elements in general. For example, just identifying the ground state of an isolated Tb atom proved to be non-trivial. Spectroscopy experiments indicate that the correct ground state is $[Xe]4f^9 6s^2$ ($J = \frac{15}{2}$) and the lowest excited state is $[Xe]4f^8 5d 6s^2$ ($J = \frac{13}{2}$) with a ≈ 0.035 eV gap [52]. Scalar relativistic AE HF calculations obtain a gap of ≈ -3.25 eV (negative, wrong ground state). Account of spin-orbit effects at the COSCI level slightly improves the

TABLE IV: Mean absolute deviations of molecular binding parameters for various core approximations with respect to AE data for $4d$ selected heavy-element groups, Y, Zr, Nb, and Rh related molecules. All parameters were obtained using Morse potential fit. The parameters shown are dissociation energy D_e , equilibrium bond length r_e , vibrational frequency ω_e and binding energy discrepancy at dissociation bond length D_{diss} .

	D_e (eV)	r_e (Å)	ω_e (cm $^{-1}$)	D_{diss} (eV)
UC	0.02(1)	0.002(2)	4(7)	0.05(8)
CRENBL	0.02(1)	0.001(2)	2(7)	0.03(8)
LANL2	0.05(1)	0.003(2)	6(7)	0.06(8)
MDFSTU	0.03(1)	0.002(2)	4(7)	0.05(8)
MWBSTU	0.01(1)	0.001(2)	3(7)	0.03(8)
SBKJC	0.03(1)	0.004(2)	10(7)	0.05(7)
ccECP	0.01(1)	0.002(2)	3(7)	0.03(8)

TABLE V: Mean absolute deviations of molecular binding parameters for various core approximations with respect to AE data for $5d$ selected heavy-element groups, Re, Ta, and Rh molecules. All parameters were obtained using Morse potential fit. The parameters shown are dissociation energy D_e , equilibrium bond length r_e , vibrational frequency ω_e and binding energy discrepancy at dissociation bond length D_{diss} .

	D_e (eV)	r_e (Å)	ω_e (cm $^{-1}$)	D_{diss} (eV)
UC	0.02(1)	0.008(5)	21(34)	0.30(12)
CRENBL	0.04(2)	0.005(5)	10(37)	0.14(11)
LANL2	0.11(2)	0.008(5)	28(38)	0.25(11)
MDFSTU	0.03(2)	0.005(5)	13(35)	0.09(11)
MWBSTU	0.04(2)	0.009(5)	29(34)	0.08(11)
SBKJC	0.07(2)	0.007(5)	35(36)	0.10(12)
ccECP	0.02(2)	0.003(5)	14(34)	0.06(11)

gap to ≈ -2.93 eV. Finally, scalar relativistic CCSD(T) obtains a ≈ -0.58 eV gap. Clearly, an accurate description of both spin-orbit effects and electron correlations is required to identify the ground state of Tb correctly. Therefore, the optimized rare-earth ccECPs open possibilities for further studies of spin-orbit effects, electron correlations, and their mutual interplay with more sophisticated approaches such as multireference CI and QMC methods.

V. CONCLUSIONS

We present a new set of correlation-consistent ECPs for selected elements Y, Zr, Nb, Rh, Ta, Re, Pt, and lanthanides, Tb, Gd. This choice has been motivated by needs from areas such as catalysis and materials research, where these elements play a prominent role. We encountered several complications that made construction much more complex than in our previous works on $5d$ transition metals[5]. This required a careful balance between

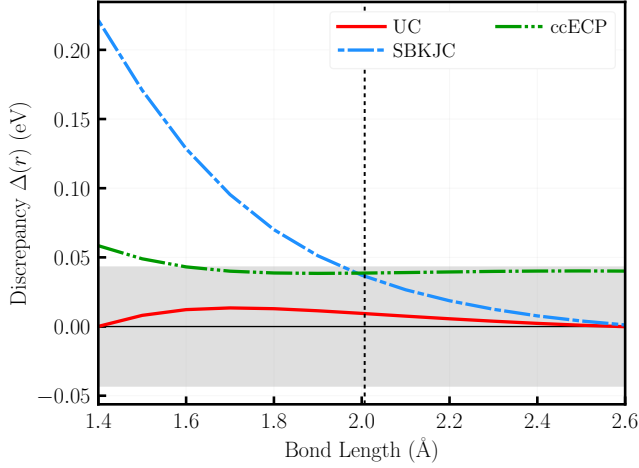
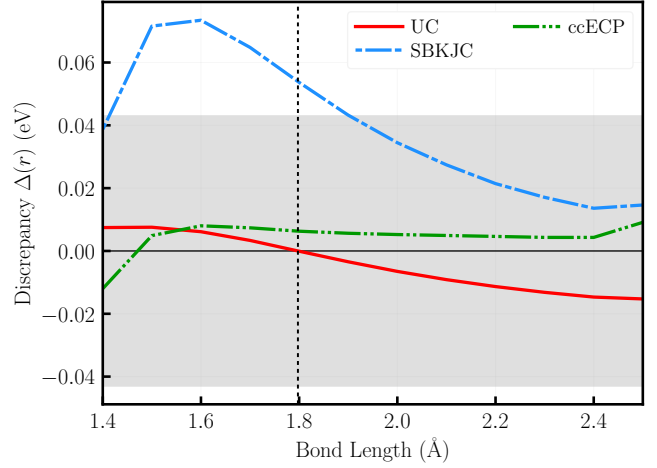
competing criteria such as fundamental accuracy, transferability in various chemical settings, efficiency in subsequent fully correlated approaches, and broad usefulness.

One of the key difficulties observed for f -elements is the near-degeneracy of $4f$ levels with s , p , and d channel states. In CCSD(T) calculations, this often results in severe convergence problems in both ECP and all electron calculations. Additionally, different choices of basis sets can also contribute to the ill-convergence behavior, with the f -elements displaying particular sensitivity to the choice of basis sets [31]. During the development, extensive efforts have been devoted to resolving such convergence and state-targeting instability issues.

We also observe that the usefulness of atomic spectra as the guiding principle of ECP constructions becomes less impactful on final quality than in previous works [1–5]. Much more significant are tests on systems with bonds due to the fact that hybridization becomes very complex and involves a large number of one-particle atomic channels due to energetic closeness of $4f$, $5d$, $6s$, and $6p$ levels. The relaxation effects and overall restructuring in these channels are substantial and difficult to predict, so the prominence of probing bonded environments grows. Indeed, this is reflected in our objective functions and makes a significant difference compared to previous constructions. This is also a significant departure from lighter elements, making the optimization more complex and demanding. The tiny biases of highly ionized states with f -occupations are negligible since their contributions in typical bonding situations become marginal, definitely well below other systematic errors involved.

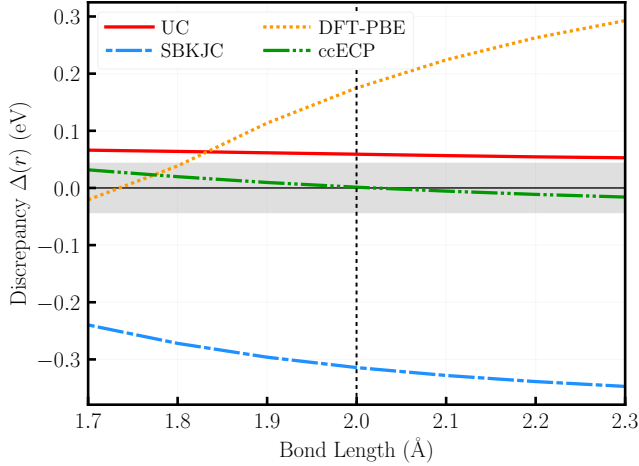
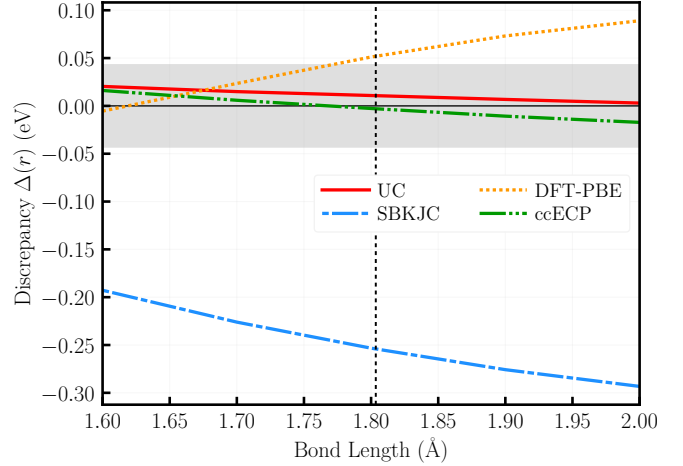
Clearly, recreating the effect of all-electron atoms with a full account of relativity, possibly QED effects, and a full account of correlation poses a significant challenge that is further complicated by effects such as core polarization and relaxation. One possible remedy would be to include core polarization and relaxation terms that have been occasionally used before. Unfortunately, this goes against the simplicity of use since almost all of the existing mainstream condensed matter codes (QUANTUM ESPRESSO, VASP) and many quantum chemistry basis set packages (PYSCF[53], GAUSSIAN[54], TURBOMOLE[55], CRYSTAL[56, 57]) do not have such terms implemented (as of this writing). We note that their inclusion in QMC codes is straightforward (a few lines of code), even in a posteriori manner, as was demonstrated a long time ago [58]. At this point, we were interested in presenting ccECPs in the same form as used for the lighter elements in order to keep the consistency and systematicity of our constructions. This leaves explorations of core relaxation and polarization effects for future work. Similarly, we plan to use the constructed effective Hamiltonians in QMC future studies so as to expand the testing and benchmarking in a variety of chemical applications.

Overall, our work provides a new generation of ECPs for selected set of heavy elements, pioneers new core-valence partitioning for $4f$ open-shell atoms, and opens possibilities for valence-only calculations with signifi-

(a) GdH₃ binding curve discrepancies

(b) GdO binding curve discrepancies

FIG. 11: Binding energy discrepancies for (a) GdH₃ and (b) GdO molecules. The grey-shaded region indicates the chemical accuracy, and the vertical dashed line gives the equilibrium bond length from the AE result.

(a) TbH₃ binding curve discrepancies

(b) TbO binding curve discrepancies

FIG. 12: Binding energy discrepancies for (a) TbH₃ and (b) TbO molecules. The grey-shaded region indicates the chemical accuracy, and the vertical dashed line gives the equilibrium bond length from the AE result. DFT-PBE is an ECP based on the Troullier-Martins scheme [50], and PBE functional [51].

cantly better account of accuracy and transparency of systematic errors involved.

VI. SUPPLEMENTARY MATERIAL

Additional information about ccECPs can be found in the Supplementary Material. Therein, AREP results for calculated atomic spectra for each element and molecular binding curve fit parameters are provided. The atomic spectra results include AE spectra for each element and the corresponding discrepancies of various core approxi-

mations. The molecular fit parameters for hydrides, trihydrides, and oxides are provided. The ccECPs in semi-local form, Kleinman-Bylander projected forms, as well as optimized Gaussian valence basis sets in various input formats (MOLPRO, GAMESS, NWCHEM) can be found on the website [59].

Concerning the SO results, the detailed atomic gaps at the COSCI (complete open-shell configuration interaction) level used for optimizing spin-orbit terms are provided.

Input and output data generated and related to this work will be published in Material Data Facility [60, 61]

and can be found in Ref.

VII. CONFLICT OF INTEREST

The authors have no conflicts to disclose.

ACKNOWLEDGMENTS

We thank Paul R. C. Kent for reading the manuscript and providing helpful suggestions.

This work has been supported by the U.S. Department of Energy, Office of Science, Basic Energy Sciences, Materials Sciences and Engineering Division, as part of the Computational Materials Sciences Program and Center for Predictive Simulation of Functional Materials.

This research used resources of the National Energy Research Scientific Computing Center (NERSC), a U.S. Department of Energy Office of Science User Facility operated under Contract No. DE-AC02-05CH11231.

An award of computer time was provided by the Innovative and Novel Computational Impact on Theory and Experiment (INCITE) program. This research used resources of the Oak Ridge Leadership Computing Facility, which is a DOE Office of Science User Facility supported under Contract No. DE-AC05-00OR22725.

This paper describes objective technical results and analysis. Any subjective views or opinions that might be expressed in the paper do not necessarily represent the views of the U.S. Department of Energy or the United States Government.

Notice: This manuscript has been authored by UT-Battelle, LLC, under contract DE-AC05-00OR22725 with the US Department of Energy (DOE). The US government retains and the publisher, by accepting the article for publication, acknowledges that the US government retains a nonexclusive, paid-up, irrevocable, worldwide license to publish or reproduce the published form of this manuscript, or allow others to do so, for US government purposes. DOE will provide public access to these results of federally sponsored research in accordance with the DOE Public Access Plan (<http://energy.gov/downloads/doe-public-access-plan>).

-
- [1] M. Chandler Bennett, Cody A. Melton, Abdulgani Annaberdiyev, Guangming Wang, Luke Shulenburger, and Lubos Mitas. A new generation of effective core potentials for correlated calculations. *J. Chem. Phys.*, 147(22):224106, December 2017.
 - [2] M. Chandler Bennett, Guangming Wang, Abdulgani Annaberdiyev, Cody A. Melton, Luke Shulenburger, and Lubos Mitas. A new generation of effective core potentials from correlated calculations: 2nd row elements. *J. Chem. Phys.*, 149(10):104108, September 2018.
 - [3] Abdulgani Annaberdiyev, Guangming Wang, Cody A. Melton, M. Chandler Bennett, Luke Shulenburger, and Lubos Mitas. A new generation of effective core potentials from correlated calculations: 3d transition metal series. *J. Chem. Phys.*, 149(13):134108, October 2018.
 - [4] Guangming Wang, Abdulgani Annaberdiyev, Cody A. Melton, M. Chandler Bennett, Luke Shulenburger, and Lubos Mitas. A new generation of effective core potentials from correlated calculations: 4s and 4p main group elements and first row additions. *J. Chem. Phys.*, 151(14):144110, October 2019.
 - [5] Guangming Wang, Benjamin Kincaid, Haihan Zhou, Abdulgani Annaberdiyev, M. Chandler Bennett, Jaron T. Krogel, and Lubos Mitas. A new generation of effective core potentials from correlated and spin-orbit calculations: Selected heavy elements. *J. Chem. Phys.*, 157(5):054101, August 2022.
 - [6] Abdulgani Annaberdiyev, Cody A. Melton, M. Chandler Bennett, Guangming Wang, and Lubos Mitas. Accurate Atomic Correlation and Total Energies for Correlation Consistent Effective Core Potentials. *J. Chem. Theory Comput.*, 16(3):1482–1502, March 2020.
 - [7] Abdulgani Annaberdiyev, Guangming Wang, Cody A. Melton, M. Chandler Bennett, and Lubos Mitas. Cohesion and excitations of diamond-structure silicon by quantum Monte Carlo: Benchmarks and control of systematic biases. *Physical Review B*, 103(20):205206, May 2021.
 - [8] Abdulgani Annaberdiyev, Cody A. Melton, Guangming Wang, and Lubos Mitas. Electronic structure of α - $RuCl_3$ by fixed-node and fixed-phase diffusion Monte Carlo methods. *Physical Review B*, 106(7):075127, August 2022.
 - [9] Cody A. Melton and Lubos Mitas. Many-body electronic structure of $LaScO_3$ by real-space quantum Monte Carlo. *Physical Review B*, 102(4):045103, July 2020.
 - [10] Xiao Wang and Timothy C. Berkelbach. Absorption Spectra of Solids from Periodic Equation-of-Motion Coupled-Cluster Theory. *Journal of Chemical Theory and Computation*, September 2021.
 - [11] Xiang Li, Cunwei Fan, Weiluo Ren, and Ji Chen. Fermionic neural network with effective core potential. *Physical Review Research*, 4(1):013021, January 2022.
 - [12] Daniel Wines, Kayahan Saritas, and Can Ataca. A first-principles Quantum Monte Carlo study of two-dimensional (2D) GaSe. *The Journal of Chemical Physics*, 153(15):154704, October 2020.
 - [13] Kenji Oqmhula, Kenta Hongo, Ryo Maezono, and Tom Ichibha. Ab initio evaluation of complexation energies for cyclodextrin drug inclusion complexes. *ACS Omega*, 5(31):19371–19376, August 2020.
 - [14] Leon Otis, Isabel Craig, and Eric Neuscamman. A hybrid approach to excited-state-specific variational Monte Carlo and doubly excited states. *The Journal of Chemical Physics*, 153(23):234105, December 2020.
 - [15] Ting Wang, Xiaojun Zhou, and Fan Wang. Performance of the Diffusion Quantum Monte Carlo Method with a Single-Slater-Jastrow Trial Wavefunction Using Natural

- Orbitals and Density Functional Theory Orbitals on Atomization Energies of the Gaussian-2 Set. *The Journal of Physical Chemistry A*, 123(17):3809–3817, May 2019.
- [16] Xiaojun Zhou, Hewang Zhao, Ting Wang, and Fan Wang. Diffusion quantum Monte Carlo calculations with a recent generation of effective core potentials for ionization potentials and electron affinities. *Phys. Rev. A*, 100(6):062502, December 2019.
- [17] Ritaj Tyagi, Andrea Zen, and Vamsee K. Voora. Quantifying the Impact of Halogenation on Intermolecular Interactions and Binding Modes of Aromatic Molecules. *The Journal of Physical Chemistry A*, 127(28):5823–5832, July 2023.
- [18] Hyeondeok Shin, Jaron T. Krogel, Kevin Gasperich, Paul R. C. Kent, Anouar Benali, and Olle Heinonen. Optimized structure and electronic band gap of monolayer GeSe from quantum Monte Carlo methods. *Physical Review Materials*, 5(2):024002, February 2021.
- [19] Adam N. Hill, Anthony J. H. M. Meijer, and J. Grant Hill. Correlation Consistent Basis Sets and Core Polarization Potentials for Al–Ar with ccECP Pseudopotentials. *The Journal of Physical Chemistry A*, 126(34):5853–5863, September 2022.
- [20] Tamar Goldzak, Xiao Wang, Hong-Zhou Ye, and Timothy C. Berkelbach. Accurate thermochemistry of covalent and ionic solids from spin-component-scaled MP2. *The Journal of Chemical Physics*, 157(17):174112, November 2022.
- [21] Adam Hassan Denawi, Fabien Bruneval, Marc Torrent, and Mauricio Rodríguez-Mayorga. *GW* density matrix to estimate self-consistent *GW* total energy in solids, June 2023.
- [22] Xia Huang, Hong Zhang, and Xin-Lu Cheng. Bandgaps in free-standing monolayer TiO₂: Ab initio diffusion quantum Monte Carlo study. *International Journal of Quantum Chemistry*, 121(12):e26643, 2021.
- [23] Benjamin Kincaid, Guangming Wang, Haihan Zhou, and Lubos Mitas. Correlation consistent effective core potentials for late 3d transition metals adapted for plane wave calculations. *The Journal of Chemical Physics*, 157(17):174307, November 2022.
- [24] M. Dolg, H. Stoll, and H. Preuss. Energy-adjusted pseudopotentials for the rare earth elements. *The Journal of Chemical Physics*, 90(3):1730–1734, February 1989.
- [25] M. Dolg and H. Stoll. Pseudopotential study of the rare earth monohydrides, monoxides and monofluorides. *Theoret. Chim. Acta*, 75(5):369–387, September 1989.
- [26] M. Dolg, H. Stoll, and H. Preuss. A combination of quasirelativistic pseudopotential and ligand field calculations for lanthanoid compounds. *Theoret. Chim. Acta*, 85(6):441–450, June 1993.
- [27] John K. Gibson. Role of Atomic Electronics in f-Element Bond Formation: Bond Energies of Lanthanide and Actinide Oxide Molecules. *The Journal of Physical Chemistry A*, 107(39):7891–7899, October 2003.
- [28] Michael Hülsen, Anna Weigand, and Michael Dolg. Quasirelativistic energy-consistent 4f-in-core pseudopotentials for tetravalent lanthanide elements. *Theor Chem Account*, 122(1):23–29, January 2009.
- [29] Jun-Bo Lu, David C. Cantu, Manh-Thuong Nguyen, Jun Li, Vassiliki-Alexandra Glezakou, and Roger Rousseau. Norm-Conserving Pseudopotentials and Basis Sets To Explore Lanthanide Chemistry in Complex Environments. *Journal of Chemical Theory and Computation*, 15(11):5987–5997, November 2019.
- [30] Jun-Bo Lu, Xue-Lian Jiang, Han-Shi Hu, and Jun Li. Norm-Conserving 4f-in-Core Pseudopotentials and Basis Sets Optimized for Trivalent Lanthanides (Ln = Ce–Lu). *Journal of Chemical Theory and Computation*, December 2022.
- [31] Charles W. Bauschlicher. The reliability of the small-core lanthanide effective core potentials. *Theoretical Chemistry Accounts*, 141(3):11, February 2022.
- [32] WMC Foulkes, Lubos Mitas, RJ Needs, and Guna Rajagopal. Quantum monte carlo simulations of solids. *Reviews of Modern Physics*, 73(1):33, 2001.
- [33] Michał Lesiuk. Implementation of the coupled-cluster method with single, double, and triple excitations using tensor decompositions. *Journal of Chemical Theory and Computation*, 16(1):453–467, 2020. PMID: 31715103.
- [34] Abdulgani Annaberdiyev, Lubos Mitas, Jaron T. Krogel, and Panchapakesan Ganesh. The role of electron correlations in the electronic structure of putative Chern magnet TbMn₆Sn₆ using correlated methods, February 2023.
- [35] Thierry Leininger, Andreas Berning, Andreas Nicklass, Hermann Stoll, Hans-Joachim Werner, and Heinz-Jürgen Flad. Spin-orbit interaction in heavy group 13 atoms and TlAr. *Chemical Physics*, 217(1):19–27, April 1997.
- [36] Hermann Stoll, Bernhard Metz, and Michael Dolg. Relativistic energy-consistent pseudopotentials—Recent developments. *J. Comput. Chem.*, 23(8):767–778, 2002.
- [37] M. Burkatzki, Claudia Filippi, and M. Dolg. Energy-consistent small-core pseudopotentials for 3d-transition metals adapted to quantum Monte Carlo calculations. *J. Chem. Phys.*, 129(16):164115, October 2008.
- [38] Walter C. Ermler, Yoon S. Lee, Phillip A. Christiansen, and Kenneth S. Pitzer. Ab initio effective core potentials including relativistic effects. a procedure for the inclusion of spin-orbit coupling in molecular wavefunctions. *Chemical Physics Letters*, 81(1):70–74, 1981.
- [39] Yoon S. Lee, Walter C. Ermler, and Kenneth S. Pitzer. Abinitio effective core potentials including relativistic effects. I. Formalism and applications to the Xe and Au atoms. *The Journal of Chemical Physics*, 67(12):5861–5876, 08 2008.
- [40] Peter Spellucci. Donlp2 nonlinear optimization code, 2009.
- [41] D. ANDRAE, U. HAUSSERMANN, M. DOLG, H. STOLL, and H. PREUSS. Energy-adjusted abinitio pseudopotentials for the 2nd and 3rd row transition-elements. *Theoretica chimica acta*, 77(2):123–141, 1990.
- [42] Kirk A. Peterson, Detlev Figgen, Michael Dolg, and Hermann Stoll. Energy-consistent relativistic pseudopotentials and correlation consistent basis sets for the 4d elements y-pd. *The Journal of chemical physics*, 126(12):124101–124101, 2007.
- [43] Detlev Figgen, Kirk A. Peterson, Michael Dolg, and Hermann Stoll. Energy-consistent pseudopotentials and correlation consistent basis sets for the 5d elements hf-pt. *The Journal of chemical physics*, 130(16):164108–164108, 2009.
- [44] L. A. LAJOHN, P. A. CHRISTIANSEN, R. B. ROSS, T. ATASHROO, and W. C. ERMLER. Ab initio relativistic effective potentials with spin-orbit operators. iii: Rb through xe. *J. Chem. Phys.; (United States)*, 87(5):2812–2824, 1987.

- [45] R. B. ROSS, J. M. POWERS, T. ATASHROO, W. C. ERMLER, L. A. LAJOHN, and P. A. CHRISTIANSEN. Ab initio relativistic effective potentials with spin-orbit operators. iv, cs through rn. *The Journal of chemical physics*, 93(9):6654–6670, 1990.
- [46] Walter J. Stevens, Morris Krauss, Harold Basch, and Paul G. Jasien. Relativistic compact effective potentials and efficient, shared-exponent basis sets for the third-, fourth-, and fifth-row atoms. *Canadian journal of chemistry*, 70(2):612–630, 1992.
- [47] Thomas R. Cundari and Walter J. Stevens. Effective core potential methods for the lanthanides. *The Journal of Chemical Physics*, 98(7):5555–5565, April 1993.
- [48] Willard R. Wadt and P. J. Hay. Ab initio effective core potentials for molecular calculations. potentials for main group elements na to bi. *J. Chem. Phys.; (United States)*, 82(1):284–298, 1985.
- [49] M. Dolg, U. Wedig, H. Stoll, and H. Preuss. Energy-adjusted ab initio pseudopotentials for the first row transition elements. *J. Chem. Phys.*, 86(2):866–872, January 1987.
- [50] N. Troullier and José Luís Martins. Efficient pseudopotentials for plane-wave calculations. *Physical Review B*, 43(3):1993–2006, January 1991.
- [51] John P. Perdew, Kieron Burke, and Matthias Ernzerhof. Generalized Gradient Approximation Made Simple. *Physical Review Letters*, 77(18):3865–3868, October 1996.
- [52] A. Kramida, Yu. Ralchenko, J. Reader, and and NIST ASD Team. NIST Atomic Spectra Database (ver. 5.10), [Online]. Available: <https://physics.nist.gov/asd> [2023, August 2]. National Institute of Standards and Technology, Gaithersburg, MD., 2022.
- [53] Qiming Sun, Timothy C. Berkelbach, Nick S. Blunt, George H. Booth, Sheng Guo, Zhendong Li, Junzi Liu, James D. McClain, Elvira R. Sayfutyarova, Sandeep Sharma, Sebastian Wouters, and Garnet Kin-Lic Chan. Pyscf: the python-based simulations of chemistry framework, 2017.
- [54] M. J. Frisch, G. W. Trucks, H. B. Schlegel, G. E. Scuseria, M. A. Robb, J. R. Cheeseman, G. Scalmani, V. Barone, G. A. Petersson, H. Nakatsuji, X. Li, M. Caricato, A. V. Marenich, J. Bloino, B. G. Janesko, R. Gomperts, B. Mennucci, H. P. Hratchian, J. V. Ortiz, A. F. Izmaylov, J. L. Sonnenberg, D. Williams-Young, F. Ding, F. Lipparini, F. Egidi, J. Goings, B. Peng, A. Petrone, T. Henderson, D. Ranasinghe, V. G. Zakrzewski, J. Gao, N. Rega, G. Zheng, W. Liang, M. Hada, M. Ehara, K. Toyota, R. Fukuda, J. Hasegawa, M. Ishida, T. Nakajima, Y. Honda, O. Kitao, H. Nakai, T. Vreven, K. Throssell, J. A. Montgomery, Jr., J. E. Peralta, F. Ogliaro, M. J. Bearpark, J. J. Heyd, E. N. Brothers, K. N. Kudin, V. N. Staroverov, T. A. Keith, R. Kobayashi, J. Normand, K. Raghavachari, A. P. Rendell, J. C. Burant, S. S. Iyengar, J. Tomasi, M. Cossi, J. M. Millam, M. Klene, C. Adamo, R. Cammi, J. W. Ochterski, R. L. Martin, K. Morokuma, O. Farkas, J. B. Foresman, and D. J. Fox. Gaussian¹⁶ Revision C.01, 2016. Gaussian Inc. Wallingford CT.
- [55] TURBOMOLE V7.2 2017, a development of University of Karlsruhe and Forschungszentrum Karlsruhe GmbH, 1989-2007, TURBOMOLE GmbH, since 2007; available from <http://www.turbomole.com>.
- [56] Alessandro Erba, Jacques K. Desmarais, Silvia Casassa, Bartolomeo Civalleri, Lorenzo Donà, Ian J. Bush, Barry Searle, Lorenzo Maschio, Loredana Edith-Daga, Alessandro Cossard, Chiara Ribaldone, Eleonora Ascritti, Nariara L. Marana, Jean-Pierre Flament, and Bernard Kirtman. Crystal23: A program for computational solid state physics and chemistry. *Journal of Chemical Theory and Computation*, 0(0):null, 0. PMID: 36502394.
- [57] Roberto Dovesi, Fabien Pascale, Bartolomeo Civalleri, Klaus Doll, Nicholas M. Harrison, Ian Bush, Philippe D’Arco, Yves Noël, Michel Rérat, Philippe Carbonnière, Mauro Causà, Simone Salustro, Valentina Lacivita, Bernard Kirtman, Anna Maria Ferrari, Francesco Silvio Gentile, Jacopo Baima, Mauro Ferrero, Raffaella Demichelis, and Marco De La Pierre. The CRYSTAL code, 1976–2020 and beyond, a long story. *The Journal of Chemical Physics*, 152(20):204111, 05 2020.
- [58] Eric L. Shirley, Luboš Mitáš, and Richard M. Martin. Core-valence partitioning and quasiparticle pseudopotentials. *Physical Review B*, 44(7):3395–3398, August 1991.
- [59] Pseudopotential Library: A community website for pseudopotentials/effective core potentials developed for high accuracy correlated many-body methods such as quantum Monte Carlo and quantum chemistry. <https://pseudopotentiallibrary.org>. Accessed: 2023-08-02.
- [60] B. Blaiszik, K. Chard, J. Pruyne, R. Ananthakrishnan, S. Tuecke, and I. Foster. The Materials Data Facility: Data Services to Advance Materials Science Research. *JOM*, 68(8):2045–2052, August 2016.
- [61] Ben Blaiszik, Logan Ward, Marcus Schwarting, Jonathon Gaff, Ryan Chard, Daniel Pike, Kyle Chard, and Ian Foster. A data ecosystem to support machine learning in materials science. *MRS Communications*, 9(4):1125–1133, December 2019.